Energy Technology
Generation, Conversion, Storage, Distribution
www.entechnol.de

Electrochemical Properties of Layered $Na_xNi_{x/2}Mn_{1-x/2}O_2$ ($0.5 \leq x \leq 1.1$) with P3 Structure as Cathode for Sodium-Ion Batteries

Liangtao Yang, Yanan Sun, and Philipp Adelhelm**

The Na properties of Ni and Mn containing layered oxides of the type $Na_xNi_{x/2}Mn_{1-x/2}O_2$ are explored between Na contents of $0.5 \leq x \leq 1.1$. Charge balance is maintained by adjusting the Ni/Mn ratio. X-ray diffraction and scanning electron microscopy are used to characterize the structure and morphology. The primary phase for all as-synthesized materials is P3, especially at Na contents below $x \leq 0.8$. Samples with a Na content of $x \geq 0.9$ lead to the formation of Na and Ni secondary phases. The Na storage properties are studied in half cells with two different voltage windows between 1.5–4.0 V and 2.2–4.5 V (vs Na^+/Na). Ni and Mn redox are active between 1.5 and 4.0 V accompanying three voltage plateaus at 3.7, 3.0, and 2.1 V, respectively. An additional high-voltage plateau (>4.0 V) is observed when increasing the cutoff voltage to 4.5 V. The initial Na content has a strong influence on the discharge capacity which ranges from 90 mAh g^{-1} ($x = 1.1$) to 210 mAh g^{-1} ($x = 0.6$). C-rate tests up to 2C and cycle life over 150 cycles are discussed. Overall, the composition $Na_{0.6}Ni_{0.3}Mn_{0.7}O_2$ shows the most favorable properties with respect to capacity retention, rate capability, and initial Coulomb efficiency.

1. Introduction

Sodium-layered oxides (Na_xTMO_2) are the most promising and diverse class of materials for the positive electrode in sodium-ion batteries (SIBs). TM represents one or more redox active 3*d* transition metals.[1] Some redox inactive elements, such as Mg or Al, may also be added in smaller amounts to tune the properties of the material. Compared to their well-known Li counterparts, Na_xTMO_2 are chemically much more diverse, which enriches the possibilities to design new materials with tailored properties.[2] At the same time, the larger Na ion leads to a more complex phase behavior which is why the composition of Na_xTMO_2 needs to be very carefully adjusted. Depending on the Na coordination and the number of TMO_2 slab in the unit cell, Na_xTMO_2 are categorized as P2, P3, O2, O3 structures, where P and O represent the prismatic (P) and octahedral (O) coordination of Na ions, respectively.[3] The structure of these materials is determined by the TMO_2 and NaO_6 interlayer electrostatic repulsion. P2 phase has two Na sites (namely, Na_e and Na_f) which are destabilized by the TMO_2—Na_eO_6 and Na_f—Na_f repulsions. O3 phase with $x = 1$ and P3 phase with $x = 0.5$ have reduced repulsion compared to P2 phase, owing to the ordering of Na ions that minimized Na—Na repulsion.[4] Thus, P3 and O3 are rather the more stable structures (with reduced repulsion). In terms of electrochemical properties, the O3 phase, in general, shows better cycling stability and the P2 phase possesses a relatively higher specific capacity (discharge capacity). Since the O2 phase is difficult to be synthesized directly by a simple chemical method (electrochemical ion exchange is possible), it is seldom applied in SIBs. In contrast, the P3 phase exhibits a comparable discharge capacity and is easy to prepare. An example is $Na_{0.5}Ni_{0.25}Mn_{0.75}O_2$,[4a,5] however, the initial charge capacity is low due to the low Na content. Recently, strategies were explored to further improve the electrochemical performances.[6] Zou et al. reported that the anion (ClO_4^-) from the electrolyte also participates the electrochemical process in P3-$Na_{0.5}Ni_{0.25}Mn_{0.75}O_2$. In this way, the electrochemical performance is enhanced.[7] Hasa et al. also explored the electrochemical properties of Ti-substituted P3 materials.[8] Recently, Zhao et al. synthesized the $LaNa_{0.06}Co_{0.06}Mn_{0.88}O_3$/$Na_{0.56}Co_{0.17}Mn_{0.8}La_{0.03}O_2$ that showed good rate performance and cycling life.[9] They also studied the electrochemical performance of the $Na_{0.67}Ni_{0.2}Co_{0.2}Mn_{0.6}O_2$ electrode.[10] However, improving the initial charge capacity of this low initial

L. Yang, Y. Sun, P. Adelhelm
Institute of Chemistry
Humboldt-University Berlin
12489 Berlin, Germany
E-mail: liangtao.yang@siat.ac.cn; philipp.adelhelm@hu-berlin.de

L. Yang
Shenzhen Institute of Advanced Technology
Chinese Academy of Sciences
Shenzhen 518055, China

P. Adelhelm
Joint research group CE-GOBA
Helmholtz-Zentrum Berlin für Materialien und Energie (HZB)
12489 Berlin, Germany

The ORCID identification number(s) for the author(s) of this article can be found under https://doi.org/10.1002/ente.202101121.

DOI: 10.1002/ente.202101121

Na content material is still necessary. P3 materials with higher Na content were recently reported by varying the composition, for example, $Na_{2/3}Ni_{1/4}Mg_{1/12}Mn_{2/3}O_2$, $Na_{0.9}Ni_{0.5}Mn_{0.5}O_2$, $Na_{0.6}Li_{0.2}Mn_{0.8}O_2$.[11] There is also evidence showing that adding the Na sacrificial salts (e.g., Na_2CO_3, $Na_2C_3O_5$) also plays a role in Na storage in Na_xTMO_2.[4a,12] Instead of focusing on single composition, we herein systematically explore the electrochemical properties of $Na_xNi_{x/2}Mn_{1-x/2}O_2$ for various compositions (x ranging from 0.5 to 1.1.). The structure and morphology are characterized by XRD and SEM. The Na storage properties are studied by galvanostatic cycling over 150 cycles and rate tests up to 2C (1C corresponds to 200 mA g^{-1}).

2. $Na_xNi_{x/2}Mn_{1-x/2}O_2$

The compositions of the Ni/Mn-based materials were chosen according to a simplified ternary composition diagram, see **Figure 1**. All Ni/Mn-based Na_xTMO_2 $Na_xTM_xO_2$ formally consist of Na, Ni, and Mn. For $Na_xTM_xO_2$, the crystal structure after calcination depends on the calcination temperature. Generally, lower temperatures lead to the P3 phase while higher temperatures lead to the P2 phase. It is claimed that the P3 to P2 transition requires the breaking of TM—O bonds which require a sufficiently high temperature.[13] To avoid temperature effects, all samples in this study were calcined at the same temperature (750 °C). The composition diagram is separated by dotted lines and some materials are marked by stars. $Na_{0.5}TMO_2$ is the starting material in our case. Materials with lower Na content were also studied, for example, $Na_{0.44}TMO_2$ with orthorhombic structure.[14] Although such materials can provide sufficient capacity in half cells (by incorporating excess Na from the Na counter electrode during cycling), the low initial Na content is unattractive for application. In the diagram, Na-poor compounds are found in the dark gray region. In lithium layered oxides, excess lithium ions

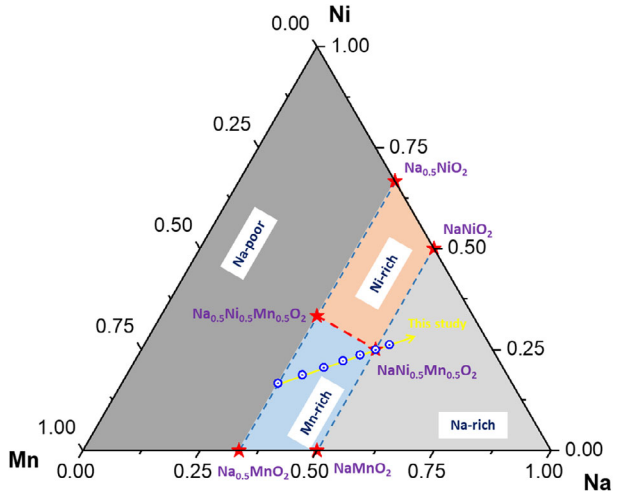

Figure 1. Ternary composition diagram for Ni/Mn-based layered oxides. The triangle is divided into four different regions, namely Na-poor, Mn-rich, Ni-rich, and Na-rich. The stars marked the selected compounds of $Na_{0.5}MnO_2$, $NaMnO_2$, $Na_{0.5}Ni_{0.5}Mn_{0.5}O_2$, $NaNi_{0.5}Mn_{0.5}O_2$, $Na_{0.5}NiO_2$, and $NaNiO_2$. The blue dot-circles indicate the compositions that will be discussed in this report.

(0.76 Å, CN = 6) can easily occupy TM sites in the TMO_2 layers, owing to the similar ionic sizes between lithium ions and many transition metal ions, e.g., $Li(Li_xNi_yCo_zMn_{1-x-y-z})O_2$ ($0 < x < 0.2$ compounds.[15] The sodium ion ($r = 1.02$ Å, CN = 6) is generally too large to occupy transition metal sites, except for Ru, Ir.[16] The light gray area in the composition diagram indicates the region when excess Na source is added (>1.0, per unit formulae), denoted as Na-rich region. Based on that, we, therefore, chose a range between $0.5 \leq Na \leq 1.1$ in this study, which is marked as an arrow in the composition diagram. According to the Ni/Mn ratio, the diagram is also divided into Ni-rich (orange) and Mn-rich (blue) materials. Both Ni and Mn have multiple valence states. But Mn^{3+} causes a strong Jahn–Teller distortion, which causes undesired voltage fading and electrode degradation.[17]In contrast, Ni^{2+} can provide a higher average potential. Considering these factors, we chose Ni^{2+}- and Mn^{4+}-based compositions in this study. For charge neutrality, the formula of the compounds can be given as

$$Na_x^{+I}TM1_{\frac{x}{2}}^{+II}TM2_{1-\frac{x}{2}}^{+IV}O_2 \quad (1)$$

Na and O valence states are +1 and −2, respectively. TM only corresponds to Ni or Mn in this report, but this formula fits all compounds consisting of divalent and tetravalent ions. All other divalent substituted materials can be designed according to this formula.[18] In this study, the $Na_xNi_{x/2}Mn_{1-x/2}O_2$ in which x in a range of 0.5–1.1 with the increment of 0.1 are investigated including the synthesis, morphology, and Na storage properties. Overall, $Na_xTM_xO_2$ are complex as the transition metal ions are multivalent cations and various oxidation states can occur during cycling. The combination of Mn and Ni is particularly of interest because Mn is abundant while Ni can provide a higher voltage.

3. Structural and Morphological Studies

All materials were synthesized using the same protocol with a series of stoichiometry ratios of reactants calculated by formula (1). The annealing temperature was set to 750 °C for all the compositions. **Figure 2** shows XRD patterns of all the resulting materials. The main diffractions of all materials can be assigned to a P3 phase with *R3m* symmetry. At low Na contents ($x = 0.5$), the reflections are sharp and well defined indicating a high purity P3 phase. No impurity is found for these compositions. For $x = 0.6$, 0.7, P2 and P3 phases are coexistent. The diffraction of the P2 phase in the material of $x = 0.7$ is more visible compared to the material with $x = 0.6$. The space group of the P2 phase is $P6_3/mmc$. Whether P2 or P3 forms, depends on the Na content and the synthesis conditions[19] Biphasic materials can be obtained for intermediate conditions.[20] As mentioned, the transition from P3 to P2 requires the breaking of TM—O bonds requires a higher temperature. At room temperature in electrochemical cells, a phase transformation from P3 to P2 and vice versa is energetically unlikely. As all materials were calcined at the same temperature (750 °C) the main driver for the different phases is the Na content. By increasing the Na content, the P3 phase is formed when the Na content is continuously increased to 0.8. However, a series of very weak diffractions from Na_2CO_3 can also be seen. The diffraction intensity of Na_2CO_3

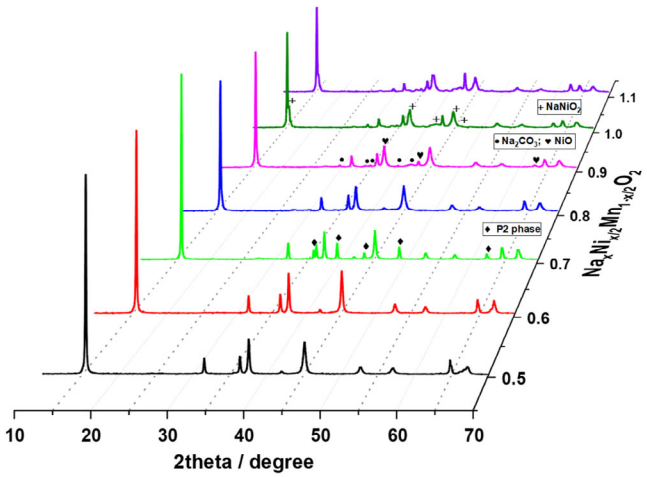

Figure 2. XRD patterns of $Na_xNi_{x/2}Mn_{1-x/2}O_2$ ($x = 0.5$, 0.6, 0.7, 0.8, 0.9, 1.0, 1.1) materials. The black vertical bars at the bottom indicate diffractions of the P3 phase (*R3m*). The black lozenges are diffractions of the P2 phase ($P6_3/mmc$) formed at $x = 0.6$–0.7. The circles, heart symbols, and plus signs are indications of Na_2CO_3, NiO, and $NaNiO_2$ impurities, respectively.

increases with increasing Na content. The Ni-containing species ($NaNiO_2$, NiO_2) are also present in the high Na content ($x = 0.9$, 1.0, 1.1) materials. **Figure 3** shows SEM images for various $Na_xNi_{x/2}Mn_{1-x/2}O_2$ compositions ($x = 0.5$, 0.7, 0.9, 1.1). Generally, the primary particles in all samples are below 1 µm, which form larger agglomerates. This small particle size is likely due to the relatively low calcination temperature.[13a] For $x = 0.7$, a secondary phase was visible in line with the appearance of secondary phases at increased Na contents. The SEM images, however, did not allow a clearer identification of the main and secondary phases.

4. Electrochemical Properties

The electrochemical properties of the different $Na_xNi_{x/2}Mn_{1-x/2}O_2$ ($x = 0.5$, 0.6, 0.7, 0.8, 0.9, 1.0, 1.1) electrodes have been studied in half cells with sodium as a counter electrode with two potential windows between 1.5–4.0 V and 2.2–4.5 V. After assembly, all cells showed an OCV of around 2.5 V. **Figure 4**a, d shows the initial charge/discharge voltage profiles for all the electrodes at C/10 rate ($C = 200\ mA\ g^{-1}$) and C/20 in the potential window of 1.5–4.0 V and 2.2–4.5 V, respectively. In both potential ranges, the electrodes with pure P3 phase ($x = 0.5$, 0.8) exhibited relatively higher initial discharge capacity compared to others. The highest discharge capacity of 208 mAh g^{-1} was delivered by the $Na_{0.6}Ni_{0.3}Mn_{0.7}O_2$ electrode, while the lowest capacity is found for $Na_{1.1}Ni_{0.55}Mn_{0.45}O_2$ (99 mAh g^{-1}). As expected, during charge, the material with the lowest Na content ($x = 0.5$) showed the lowest charge capacity under both potential windows. Moreover, this material possesses the $Ni^{2+} \rightarrow Ni^{4+}$ redox reaction under 4.0 V,[21] while the other materials exhibit a two-stage reaction of $Ni^{2+} \rightarrow Ni^{3+} \rightarrow Ni^{4+}$ accompanying two plateaus at 3.2 and 3.6 V.[10,22] When the cutoff voltage extends to 4.5 V, a high-voltage plateau is found for all compositions which are commonly found for many layered oxides. Several processes can contribute to this plateau, e.g., a P/O transition,[11b,23] the formation of new phases (OP4 and/or Z phase),[24] contributions from anionic redox of lattice oxygen ($O^{2-} \rightarrow O_2^-$)[25] or the decomposition of sodium carbonate.[4a] During discharge, there is a new plateau in all samples appearing below 2.2 V that is associated with the $Mn^{4+} \rightarrow Mn^{3+}$ reduction. The lower sodium content materials show a relatively higher Mn redox activity. This might be caused by the larger number of Na vacancies.[26] During discharge, the sodium ions from the counter electrode can occupy these free sites leading to an extra

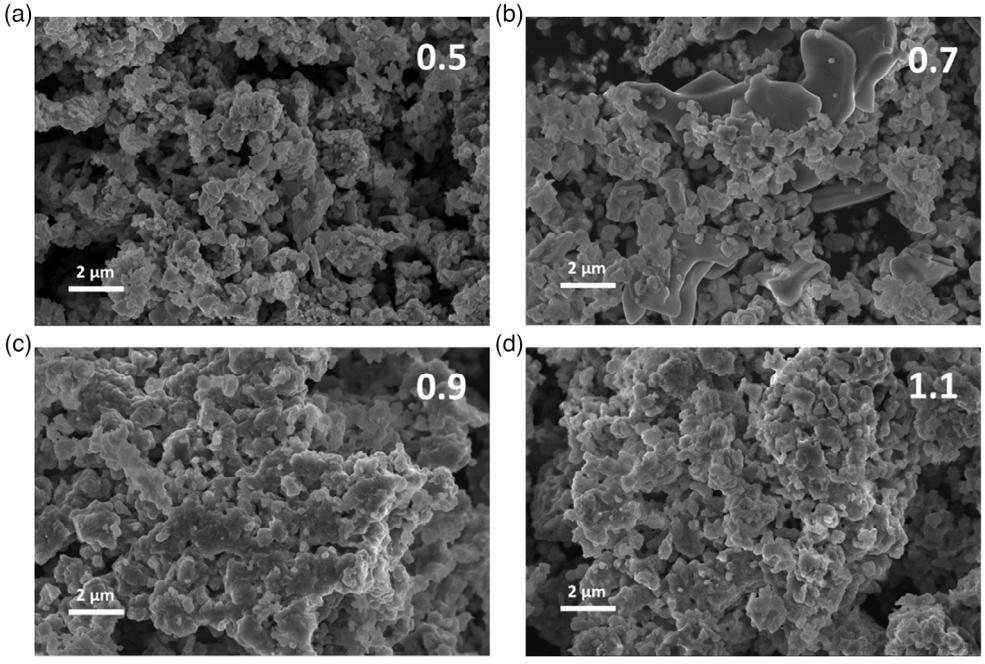

Figure 3. SEM images for $Na_xNi_{x/2}Mn_{1-x/2}O_2$ ($x =$ a) 0.5, b) 0.7, c) 0.9, and d) 1.1) materials.

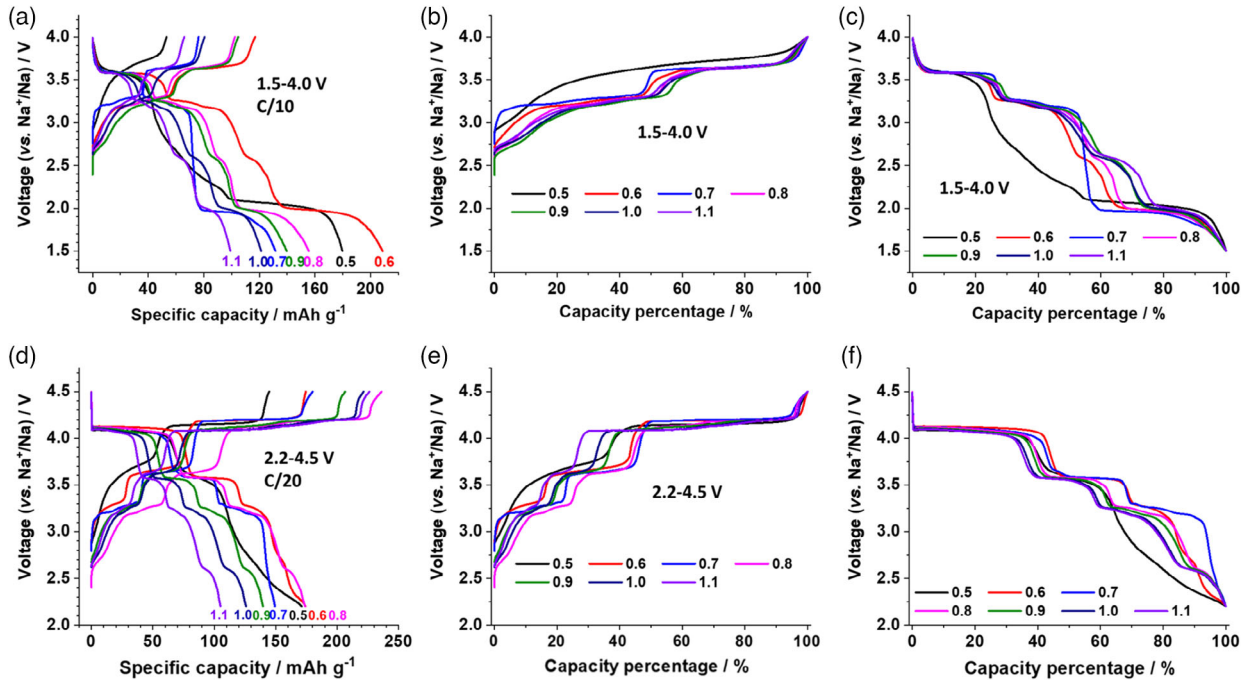

Figure 4. Galvanostatic charge–discharge voltage profiles at: a) C/10 in the voltage range 1.5–4.0 V and d) at C/20 in the voltage range 2.2–4.5 V, and b,e) the normalized charge and c,f) discharge curves for $Na_xNi_{x/2}Mn_{1-x/2}O_2$ ($x = 0.5, 0.6, 0.7, 0.8, 0.9, 1.0, 1.1$) electrodes. b), c), e), and f) were normalized with their own charge (b,e)/discharge (c,f) capacity. 1C corresponds to 200 mA g^{-1}.

capacity. As a result, the $Na_{0.5}Ni_{0.25}Mn_{0.75}O_2$ shows the largest initial Coulomb efficiency within 1.5–4.0 V, and the $Na_{1.1}Ni_{0.55}Mn_{0.45}O_2$ shows the lowest initial Coulomb efficiency within 2.2–4.5 V.

Figure 4b,c,e,f shows the normalized charge and discharge voltage curves. Since the $Na_{0.5}Ni_{0.25}Mn_{0.75}O_2$ material shows a unique redox behavior as well as a different capacity contribution, it is hard to directly compare the capacity contributions of this electrode with other studied compositions. When the voltage window is between 1.5 and 4.0 V, the charge capacity contributions are similar with almost half capacity for each stage, indicating that the $Ni^{2+}\rightarrow Ni^{3+}\rightarrow Ni^{4+}$ oxidation is not affected by the impurity and the sodium content. During discharge, the Ni capacity contribution for all samples is nearly the same. Whereas, the $Mn^{4+\rightarrow 3+}$ reduction contribution is varied. Samples with less sodium content show higher values, while the $Mn^{4+}\rightarrow Mn^{3+}$ reduction is less in these materials with higher sodium content. When the voltage window changed to 2.2–4.5 V, the materials with a sodium content of $x = 0.6, 0.7, 0.8$) contribute half capacity over 4.0 V. The materials with a sodium content of $x = 0.9, 1.0, 1.1$ have higher high-voltage (<4.0 V) capacity contribution, which is likely due to the excess sodium ions and decomposition of impurities, e.g., sodium carbonate.[4a] During discharge, high-voltage capacity contributions are less than 40%. The high-voltage discharge capacity decreases with the increase in Na content, implying poor reversibility of high-voltage redox reactions.

Rate capability tests were done at various current rates of C/10, C/4, C/2, C, 2C between 1.5 and 4.0 V and C/20, C/10, C/4, C/2, C between 2.2 and 4.5 V, as shown in **Figure 5**a,b. In the voltage range of 1.5–4.0 V, $Na_{0.6}Ni_{0.3}Mn_{0.7}O_2$ shows the highest discharge capacity at the lowest C rate (C/10), while $Na_{0.7}Ni_{0.35}Mn_{0.65}O_2$ displays the lowest capacity at the highest 2C rate around 50 mAh g^{-1}. When the operation voltage window was changed to 2.2–4.5 V, $Na_{0.6}Ni_{0.3}Mn_{0.7}O_2$ still shows the highest capacities both at the lowest rate (C/20) and highest rate (C). Nevertheless, the capacities at some rates (C/10, C/4, C/2) are lower than that of the $Na_{0.5}Ni_{0.25}Mn_{0.75}O_2$ electrode. The $Na_{1.1}Ni_{5.5}Mn_{4.5}O_2$ material shows the lowest capacities at all rates. The capacity retention over 150 cycles at C/4 within different voltage windows is shown in Figure 5c,d. The highest capacity retention is 49.2% which is found for the $Na_{0.6}Ni_{0.3}Mn_{0.7}O_2$ electrode which was cycled between 1.5 and 4.0 V. Generally, cycling the electrodes between 2.2 and 4.5 V leads to faster capacity fade compared to the 1.5–4.0 V window. This indicates that the reversibility of high-voltage plateau is lower than that of the $Mn^{4+/3+}$ redox at low voltage. The electrochemical properties for all samples are listed in **Table 1**. Overall, Ni ($Ni^{2+}\rightarrow Ni^{4+}$), $Ni^{2+}\rightarrow Ni^{3+}\rightarrow Ni^{4+}$), Mn ($Mn^{3+}\rightarrow Mn^{4+}$), and high-voltage redox are coexistent in all materials which are not related to the Na content. As expected, the initial charge capacity is negatively correlated to the Na content. As a general trend, the more well-defined the crystallinity of the material, the better the discharge capacity and capacity retention.

5. Conclusion

P3-Ni/Mn-based layered oxides ($Na_xNi_{x/2}Mn_{1-x/2}O_2$) with Na contents between $x = 0.5$ and 1.1 were synthesized to study

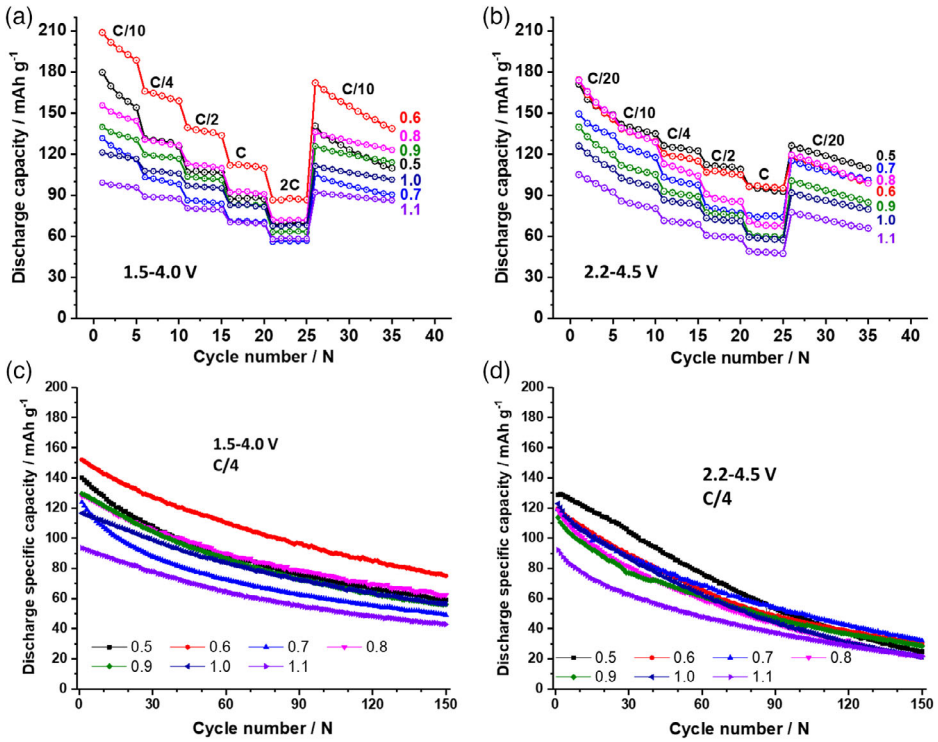

Figure 5. a,b) Rate capability for $Na_xNi_{x/2}Mn_{1-x/2}O_2$ ($x = 0.5, 0.6, 0.7, 0.8, 0.9, 1.0, 1.1$) materials. c,d) Capacity retention of all materials cycled at C/4 rate over 150 cycles. For the diagram, 1C corresponds to 200 mA g^{-1}.

Table 1. Summary of the electrochemical properties of $Na_xNi_{x/2}Mn_{1-x/2}O_2$.

$Na_xNi_{x/2}Mn_{1-x/2}O_2$								
	X=	0.5	0.6	0.7	0.8	0.9	1.0	1.1
1.5–4.0 V	First charge (C/10) [mAh g^{-1}]	53.2	177.0	76.2	102.4	104.8	80.6	66.0
	First discharge (C/10) [mAh g^{-1}]	179.7	208.7	131.6	155.6	139.8	121.2	99.1
	Discharge capacity at 2C rate [mAh g^{-1}]	69.3	87.6	50.6	71.8	63.4	67.9	58.5
	Capacity retention (C/4 over 150 cycles) [%]	42.1	49.2	39.6	48.8	43.2	48.2	45.8
2.2–4.5 V	First charge (C/20) [mAh g^{-1}]	144.7	174.6	180.1	236.1	206.6	221.3	226.3
	First discharge (C/20) [mAh g^{-1}]	171.1	174.3	149.4	174.0	139.7	125.9	105.0
	Discharge capacity at C rate [mAh g^{-1}]	94.7	95.8	74.7	67.8	59.6	58.1	48.3
	Capacity retention (C/4 over 150 cycles) [%]	19.3	25.1	26.8	18.0	25.1	17.4	23.4

the influence of the initial sodium content on the structure, morphology, and Na storage properties. It was found that low Na contents ($x = 0.5$) favor a phase pure P3 structure. For compositions with higher Na content, the P3 phase is still the dominant phase, however, secondary phases form. For $x = 0.7$, a biphasic P2/P3 material was obtained and at contents of contents of $x \geq 0.8$, sodium carbonate, and nickel oxides (NiO, $NaNiO_2$) were formed too. The electrochemical properties were investigated with respect to the rate capability and cycling stability in half cells with Na as a counter electrode. Two different voltage windows (1.5–4.0 V and 2.2–4.5 V) were applied. The materials ($x = 0.5, 0.6, 0.8$) with a high degree of crystallinity delivered relatively higher specific capacity and showed better cycle life. The highest discharge capacity was delivered by $Na_{0.6}Ni_{0.3}Mn_{0.7}O_2$ at C/10 (209 mAh g^{-1}) and at 2C (88 mAh g^{-1}) in the voltage range of 1.5–4.0 V. The best capacity retention was also obtained for this material reaching 49.2% at C/4 rate over 150 cycles. The cells cycled between 1.5 and 4.0 V had a low charge capacity but a high discharge capacity compared to the cells cycled between 2.2 and 4.5 V. This means the $Mn^{4+\rightarrow 3+}$redox at low voltage (<2.2 V) is more reversible than the high-voltage redox. It is also found that the initial charge capacity surprisingly decreases with increasing Na content which indicates that other measures such as sacrificial salts are necessary to compensate for the Na deficiency in these materials.[27] For all compositions, the capacity retention needs to be improved. This may be also reached by tests in full cells which avoid crosstalk between the Na counter electrode and $Na_xNi_{x/2}Mn_{1-x/2}O_2$. In contrast, this complicates the analysis of

the voltage profiles as the counter electrode does not provide a stable reference potential anymore. As general trends, the discharge capacity and retention are positively correlated to the degree of crystallinity. It is believed this finding will be helpful to design high-performance positive materials for SIBs.

6. Experimental Section

Materials Synthesis: The series of layered sodium oxides $Na_xNi_{x/2}Mn_{1-x/2}O_2$ ($x = 0.5, 0.6, 0.7, 0.8, 0.9, 1.0, 1.1$) were synthesized by sol–gel method followed high-temperature calcination, the same conditions have been reported in our previous work.[28] Stoichiometric amounts of $NaNO_3$, Sigma-Aldrich, ≥99%, $LiNO_3$, Alfa Aesar, ≥99%, $Ni(NO_3)_26H_2O$, Alfa Aesar, ≥99%, and $(CH_3CO_2)_2Mn{\cdot}4H_2O$, Sigma-Aldrich, ≥99%, were mixed in deionized water (0.07 μS cm^{-2}) and then stirred for 2 h before adding the chelating agent—citric acid. The solution was then kept at 100 °C under constant stirring in air until a homogeneous gel was obtained. The as-prepared gel was then dried at 500 °C for 3 h followed by annealing at 750 °C for 24 h in a Muffle oven under air. The final products were transferred into Ar-filled glovebox (MBraun, $H_20 \leq 0.1$ ppm, $O_2 \leq 0.1$ ppm) immediately to avoid contact with moisture in the air.

Material Characterization: Chemical compositions of all the layered oxide cathodes were determined by inductively coupled plasma optical emission spectrometry technique (ICP-OES, spectrometer Ultima-2 from JobinYvon Horiba). The crystalline phases of the synthesized materials were identified by powder XRD, Bruker, D2-phaser, using Cu-Kα radiation ($\lambda = 1.54056$ Å). XRD data were obtained in the 2θ range between 10° and 70° with a step width of 0.02°. The special airtight sample holder was used for the air-sensitive samples. The results were analyzed by the EVA software. The morphology of the as-prepared samples was characterized by a Sigma VP field emission scanning electron microscope (Carl-Zeiss AG, Germany).

Electrochemical Experiments: The positive electrodes were prepared by coating a slurry mixing active materials, carbon black, and polyvinylidene fluoride (PVDF) binder in *N*-methyl-2-pyrrolidone (NMP) in the weight ratio 8:1:1, onto the carbon-coated Al current collector (MTI corp.). The electrodes were dried overnight at 70 °C to evaporate the solvent. The electrodes were punched into a 12 mm Ø disc and then dried overnight at 120 °C under vacuum. The active materials loading of the electrodes were in the range of 2.2–4.5 mg cm^{-2}. Sodium (BASF) was used as the negative electrode. The electrolyte solution was 1 M $NaClO_4$ in PC/FEC (98:2) and a Whatman filter paper (CAT No. 1820-090, Whatman Corp.) as a separator. The CR2032 coin-type cells were assembled in an Ar-filled glovebox to evaluate the performance of the layered oxides. Galvanostatic charge-discharge experiments were carried out at various current densities using Bio-Logic BCS 805 multichannel battery cycler.

Acknowledgements

P.A. thanks the support within for LIBRA project within the EIG Concert Japan program financed by BMBF (01DR18003), MINECO, and JST. L.Y. thanks the China Scholarship Council for funding. The authors acknowledge Ms. S. Strumpf for the SEM images from the SEM facilities of the Jena Center for Soft Matter (JCSM) established with a grant from the German Research Council (DFG) and the European Fonds for Regional Development (EFRE).

Open access funding enabled and organized by Projekt DEAL.

Conflict of Interest

The authors declare no conflict of interest.

Data Availability Statement

The data that support the findings of this study are available from the corresponding author upon reasonable request.

Keywords

cathode materials, energy storage, layered oxides, sodium-ion batteries

Received: January 14, 2022
Published online: February 26, 2022

[1] a) R. Usiskin, Y. Lu, J. Popovic, M. Law, P. Balaya, Y.-S. Hu, J. Maier, *Nat. Rev. Mater.* **2021**, *6*, 1020; b) E. Goikolea, V. Palomares, S. Wang, I. R. de Larramendi, X. Guo, G. Wang, T. Rojo, *Adv. Energy Mater.* **2020**, *10*, 2002055; c) S. Komaba, *Electrochemistry* **2019**, *87*, 312; d) Y. E. Durmus, H. Zhang, F. Baakes, G. Desmaizieres, H. Hayun, L. Yang, M. Kolek, V. Küpers, J. Janek, D. Mandler, S. Passerini, Y. Ein-Eli, *Adv. Energy Mater.* **2020**, *10*, 2000089.

[2] a) C. Delmas, D. Carlier, M. Guignard, *Adv. Energy Mater.* **2020**, *11*, 2001201; b) P. K. Nayak, L. Yang, W. Brehm, P. Adelhelm, *Angew. Chem.* **2018**, *57*, 102.

[3] a) C. Delmas, C. Fouassier, P. Hagenmuller, *Physica* **1980**, *99B*, 81; b) C. Delmas, C. Fouassier, P. Hagenmuller, *Phys. B&C* **1980**, *99B*, 81; c) C. Delmas, *Adv. Energy Mater.* **2018**, *8*, 1703137.

[4] a) M. Sathiya, J. Thomas, D. Batuk, V. Pimenta, R. Gopalan, J.-M. Tarascon, *Chem. Mater.* **2017**, *29*, 5948; b) K. Kubota, S. Kumakura, Y. Yoda, K. Kuroki, S. Komaba, *Adv. Energy Mater.* **2018**, *8*, 1703415.

[5] M. Kalapsazova, G. F. Ortiz, J. L. Tirado, O. Dolotko, E. Zhecheva, D. Nihtianova, L. Mihaylov, R. Stoyanova, **2015**, *80*, 1642.

[6] S. Maddukuri, P. Valerie, V. V. Upadhyayula, **2017**, *2*, 5660.

[7] Q. Li, Y. Qiao, S. Guo, K. Jiang, Q. Li, J. Wu, H. Zhou, *Joule* **2018**, *2*, 1134.

[8] I. Hasa, D. Buchholz, S. Passerini, B. Scrosati, J. Hassoun, *Adv. Mater.* **2014**, *4*, 1400083.

[9] F. Xia, D. Tie, J. Wang, H. Song, W. Wen, X. Ye, J. Wu, Y. Hou, X. Lu, Y. Zhao, *Energy Storage Mater.* **2021**, *42*, 209.

[10] X. Wang, X. Yin, X. Feng, Y. Li, X. Dong, Q. Shi, Y. Zhao, J. Zhang, *Chem. Eng. J.* **2022**, *428*, 130990.

[11] a) Y.-N. Zhou, P.-F. Wang, X.-D. Zhang, L.-B. Huang, W.-P. Wang, Y.-X. Yin, S. Xu, Y.-G. Guo, *ACS Appl. Mater. Interfaces* **2019**, *11*, 24184; b) T. Risthaus, L. Chen, J. Wang, J. Li, D. Zhou, L. Zhang, D. Ning, X. Cao, X. Zhang, G. Schumacher, M. Winter, E. Paillard, J. Li, *Chem. Mater.* **2019**, *31*, 5376; c) X. Rong, J. Liu, E. Hu, Y. Liu, Y. Wang, J. Wu, X. Yu, K. Page, Y.-S. Hu, W. Yang, H. Li, X.-Q. Yang, L. Chen, X. Huang, *Joule* **2018**, *2*, 125.

[12] A. J. Fernández-Ropero, M. Zarrabeitia, G. Baraldi, M. Echeverria, T. Rojo, M. Armand, D. Shanmukaraj, *ACS Appl. Mater. Interfaces* **2021**, *13*, 11814.

[13] a) K. Kubota, S. Kumakura, Y. Yoda, K. Kuroki, S. Komaba, *Adv. Energy Mater.* **2018**, *8*, 1703415; b) S. Guo, Y. Sun, J. Yi, K. Zhu, P. Liu, Y. Zhu, G.-Z. Zhu, M. Chen, M. Ishida, H. Zhou, *NPG Asia Mater.* **2016**, *8*, 266.

[14] a) X. He, J. Wang, B. Qiu, E. Paillard, C. Ma, X. Cao, H. Liu, M. C. Stan, H. Liu, T. Gallash, Y. S. Meng, J. Li, *Nano Energy* **2016**, *27*, 602; b) N. Sheng, C.-G. Han, Y. Lei, C. Zhu, *Electrochim. Acta* **2018**, *283*, 1560; c) V. Dall'Asta, D. Buchholz, L. G. Chagas, X. Dou, C. Ferrara, E. Quartarone, C. Tealdi, S. Passerini, *ACS Appl. Mater. Interfaces* **2017**, *9*, 34891.

[15] a) P. Rozier, J. M. Tarascon, *J. Electrochem. Soc.* **2015**, *162*, A2490; b) B. Qiu, M. Zhang, Y. Xia, Z. Liu, Y. S. Meng, *Chem. Mater.* **2017**, *29*, 908.

[16] a) M. Tamaru, X. Wang, M. Okubo, A. Yamada, *Electrochem. Commun.* **2013**, *33*, 23; b) D. D. Gazizova, A. V. Ushakov, S. V. Streltsov, *JETP Lett.* **2018**, *107*, 483; c) B. Mortemard de Boisse, G. Liu, J. Ma, S.-I. Nishimura, S.-C. Chung, H. Kiuchi, Y. Harada, J. Kikkawa, Y. Kobayashi, M. Okubo, A. Yamada, *Nat. Commun.* **2016**, *7*, 11397; d) A. J. Perez, D. Batuk, M. Saubanère, G. Rousse, D. Foix, E. McCalla, E. J. Berg, R. Dugas, K. H. W. van den Bos, M.-L. Doublet, D. Gonbeau, A. M. Abakumov, G. Van Tendeloo, J.-M. Tarascon, *Chem. Mater.* **2016**, *28*, 8278.

[17] a) L. Yang, Y. Xia, X. Fan, L. Qin, B. Qiu, Z. Liu, *Electrochim. Acta* **2016**, *191*, 200; b) K. Zhang, D. Kim, Z. Hu, M. Park, G. Noh, Y. Yang, J. Zhang, V. W.-H. Lau, S.-L. Chou, M. Cho, S.-Y. Choi, Y.-M. Kang, *Nat. Commun.* **2019**, *10*, 5203.

[18] a) U. Maitra, R. A. House, J. W. Somerville, N. Tapia-Ruiz, J. G. Lozano, N. Guerrini, R. Hao, K. Luo, L. Jin, M. A. Perez-Osorio, F. Massel, D. M. Pickup, S. Ramos, X. Lu, D. E. McNally, A. V. Chadwick, F. Giustino, T. Schmitt, L. C. Duda, M. R. Roberts, P. G. Bruce, *Nat. Chem.* **2018**, *10*, 288; b) R. J. Clément, J. Billaud, A. Robert Armstrong, G. Singh, T. Rojo, P. G. Bruce, C. P. Grey, *Energy Environ. Sci.* **2016**, *9*, 3240.

[19] Y. Lei, X. Li, L. Liu, G. Ceder, *Chem. Mater.* **2014**, *26*, 5288.

[20] a) E. Lee, J. Lu, Y. Ren, X. Luo, X. Zhang, J. Wen, D. Miller, A. DeWahl, S. Hackney, B. Key, D. Kim, M. D. Slater, C. S. Johnson, *Adv. Energy Mater.* **2014**, *4*, 1400458; b) M. Bianchini, E. Gonzalo, N. E. Drewett, N. Ortiz-Vitoriano, J. M. López del Amo, F. J. Bonilla, B. Acebedo, T. Rojo, *J. Mater. Chem. A* **2018**, *6*, 3552; c) Z.-Y. Li, J. Zhang, R. Gao, H. Zhang, L. Zheng, Z. Hu, X. Liu, *J. Phys. Chem. C* **2016**, *120*, 9007.

[21] a) P. Manikandan, D. Ramasubramonian, M. M. Shaijumon, *Electrochim. Acta* **2016**, *206*, 199; b) J. Yang, T. Yuan, B. Guo, C. Dai, Y. Liu, G. Li, G. Liu, M. Xu, *Chem. Commun.* **2017**, *53*, 9117; c) Z.-Y. Li, X. Ma, K. Sun, L. He, Y. Li, D. Chen, *ACS Appl. Energy Mater.* **2021**, *5*, 1126.

[22] a) J. Alvarado, C. Ma, S. Wang, K. Nguyen, M. Kodur, Y. S. Meng, *ACS Appl. Mater. Interfaces* **2017**, *9*, 26518; b) Q. Liu, Z. Hu, M. Chen, C. Zou, H. Jin, S. Wang, Q. Gu, S. Chou, *J. Mater. Chem. A* **2019**, *7*, 9215.

[23] a) X. Wu, G.-L. Xu, G. Zhong, Z. Gong, M. J. McDonald, S. Zheng, R. Fu, Z. Chen, K. Amine, Y. Yang, *ACS Appl. Mater. Interfaces* **2016**, *8*, 22227; b) P.-F. Wang, Y. You, Y.-X. Yin, Y.-S. Wang, L.-J. Wan, L. Gu, Y.-G. Guo, *Angew. Chem. Int. Ed.* **2016**, *55*, 7445.

[24] a) N. Yabuuchi, M. Kajiyama, J. Iwatate, H. Nishikawa, S. Hitomi, R. Okuyama, R. Usui, Y. Yamada, S. Komaba, *Nat. Mater.* **2012**, *11*, 512; b) N. A. Katcho, J. Carrasco, D. Saurel, E. Gonzalo, M. Han, F. Aguesse, T. Rojo, *Adv. Energy Mater.* **2017**, *7*, 1601477; c) J. W. Somerville, A. Sobkowiak, N. Tapia-Ruiz, J. Billaud, J. G. Lozano, R. A. House, L. C. Gallington, T. Ericsson, L. Häggström, M. R. Roberts, U. Maitra, P. G. Bruce, *Energy Environ. Sci.* **2019**, *12*, 2223; d) E. Talaie, V. Duffort, H. L. Smith, B. Fultz, L. F. Nazar, *Energy Environ. Sci.* **2015**, *8*, 2512.

[25] a) X. Rong, E. Hu, Y. Lu, F. Meng, C. Zhao, X. Wang, Q. Zhang, X. Yu, L. Gu, Y.-S. Hu, H. Li, X. Huang, X.-Q. Yang, C. Delmas, L. Chen, *Joule* **2019**, *3*, 503; b) D. Kim, M. Cho, K. Cho, *Adv. Mater.* **2017**, *29*, 1701788; c) C. Zhao, Q. Wang, Y. Lu, Y.-S. Hu, B. Li, L. Chen, *J. Phys. D: Appl. Phys.* **2017**, *50*, 183001.

[26] a) J. S. Thorne, R. A. Dunlap, M. N. Obrovac, *J. Electrochem. Soc.* **2012**, *160*, A361; b) L. Yang, L.-Y. Kuo, J. M. López del Amo, P. K. Nayak, K. A. Mazzio, S. Maletti, D. Mikhailova, L. Giebeler, P. Kaghazchi, T. Rojo, P. Adelhelm, *Adv. Funct. Mater.* **2021**, *31*, 2102939.

[27] F. Xie, Y. Lu, L. Chen, Y.-S. Hu, *Chin. Phys. Lett.* **2021**, *38*, 118401.

[28] P. K. Nayak, L. Yang, K. Pollok, F. Langenhorst, L. Wondraczek, P. Adelhelm, *Batteries Supercaps* **2018**, *2*, 104.